

# MEMS sensor material based on polypyrrole–carbon nanotube nanocomposite: film deposition and characterization

Kwok-Siong Teh and Liwei Lin

Berkeley Sensors and Actuators Center, Department of Mechanical Engineering,  
University of California, 497 Cory Hall, Berkeley, CA, USA

E-mail: [kwok.siong@gmail.com](mailto:kwok.siong@gmail.com)

Received 12 April 2005, in final form 15 July 2005

Published 20 September 2005

Online at [stacks.iop.org/JMM/15/2019](http://stacks.iop.org/JMM/15/2019)

## Abstract

Conductive polymer-based nanocomposite has been utilized as a MEMS sensing material via a one-step, selective on-chip deposition process at room temperature. A doped polypyrrole (PPy) variant synthesized by incorporating multi-walled carbon nanotube (MWCNT) into electropolymerized PPy has been shown to improve the sensing performance utilizing a two-terminal, micro-gap chemiresistor architecture. The dodecylbenzenesulfonate (DBS)-doped PPy–MWCNT nanocomposites are found to be responsive to oxidants, such as hydrogen peroxide ( $\text{H}_2\text{O}_2$ ), and this effect can be extended to glucose detection using  $\text{H}_2\text{O}_2$  as a proxy material. The oxidant sensing effect is demonstrated by subjecting a glucose oxidase (GOx)-laden PPy–MWCNT nanocomposite film to various concentrations of glucose solution. Such PPy–MWCNT nanocomposite, when applied in a chemiresistor configuration, obviates the need for reference electrode and electron mediators, by measuring the direct and reversible, oxidation–reduction induced conductivity change. Experimentally, GOx-laden, doped PPy–MWCNT is tested to be sensitive to glucose concentration up to 20 mM, which covers the physiologically important range for diabetics of 0–20 mM.

(Some figures in this article are in colour only in the electronic version)

## 1. Introduction

Relentless miniaturization of portable systems creates unique opportunities to expand the microsensors technologies. Without doubt, sensing material represents one of the key elements in microsensors developments. This work investigates and integrates conductive polymer/nanomaterials technologies with MEMS processes for sensing applications with two potential distinctive advantages over other approaches: (1) CMOS-compatible material deposition process for large-scale integration and (2) multi-functional and site-specific detection utilizing different nanocomposite materials at different detection positions on a single chip.

Previously, Smela *et al* have performed a significant amount of work on characterizing microactuators made of an environmentally stable conductive polymer, sodium dodecylbenzenesulfonate (NaDBS)-doped PPy [1, 2]. PPy is one of the most researched conductive polymers because of its environmental stability and unique properties such as biocompatibility [3], redox-tunable conductivity and ease of processibility. In the absence of dopant, pristine PPy or  $\text{PPy}^0$  ( $E_g \sim 3.2$  eV) is an insulator and has a benzoid structure [4]. However, once it is doped, it functions as a polymeric semiconducting material whose conductivity can be altered to varying extents via the incorporation of anionic dopants such as perchlorate ( $\text{ClO}_4^-$ ), tetrafluoroborate ( $\text{BF}_4^-$ ), sulfate

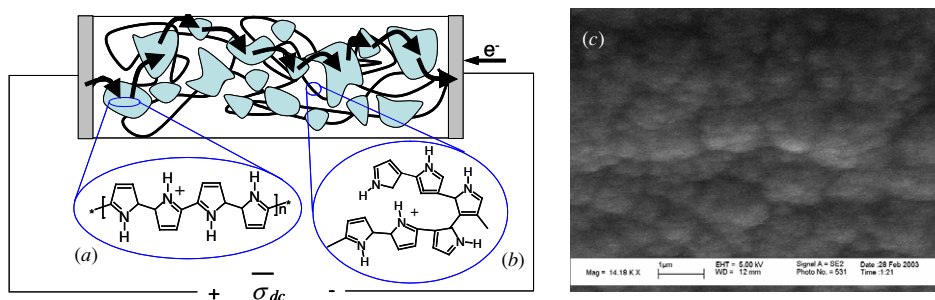


**Figure 1.** A general scheme of polypyrrole (PPy) conduction. The shaded patches (a) indicate the conductive region and the solid curve (b) shows the insulating region. Charge transport proceeds through a ‘hopping’ mechanism (as indicated by the arrows) from the positive to the negative terminal. (c) SEM of an as-deposited PPy film in this work.

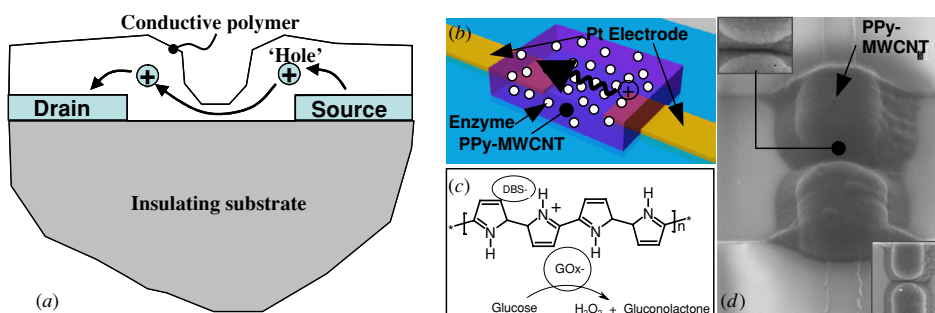


**Figure 2.** (a) A conductimetric sensor consists of a pair of electrodes joined by a conductive polymer. Secondary dopant effect, e.g. redox gases, causes conductivity change. (b) Schematic of a PPy-MWCNT glucose sensor. (c) A DBS-doped PPy-MWCNT with GOx embedded will oxidize glucose to produce  $H_2O_2$  and gluconolactone and enhance the conductivity of PPy-MWCNT. (d) Oblique SEM of a fabricated PPy-MWCNT sensor. Top and bottom insets show the bridged micro-gap and the top view of the sensor, respectively.

( $SO_4^-$ ), chloride ( $Cl^-$ ), dodecylbenzenesulfonate ( $DBS^-$ ) and *p*-toluenesulfonate ( $PTS^-$ ) [5, 6]. Additionally, depending on the charge and size of the specific dopant added, the conductivity may be reversibly modulated by external parameters such as temperature and pressure [7], as well as by ‘secondary dopants’ such as water molecules [8], protons [9] and reducing/oxidizing gaseous molecules ( $NH_3$ ,  $I_2$ ) [10, 11].

Unlike metals, PPy (as with all conductive polymers) is still very much sensitive to the environment and its electrical properties tend to deteriorate over time due to an irreversible oxidative degradation process commonly referred to as ‘overoxidation’ [12], mechanical perturbation, elevated temperature and chemical alteration (such as deprotonation and nucleophilic attack initiated by strong bases). Most doped PPy are poorly crystalline materials and there is a wide distribution of conjugation lengths with the long conjugated segments being more easily oxidized than the short conjugated segments [13]. This sensitivity to oxidation significantly influences its charge transport mechanism, as depicted by a simplified model in figure 1. As-polymerized and doped PPy consists of a random mixture of conducting (semi-crystalline) domains as represented by the shaded area in figure 1(a) and insulating (amorphous) domains as represented by the solid lines in figure 1(b). Upon the injection of a hole from external sources, a defect in the polymer chain (‘polaron’) is created [4]. If an electric potential is applied, the polaron is able to propagate along and between the chains (interchain) via a ‘hopping’ mechanism, where the polarons hop over islands of insulating domains. Figure 1(c) shows an as-deposited PPy

film from this work with doped NaDBS using a +0.6 V bias during the deposition process at room temperature.

This paper explores two materials: (1) NaDBS-doped PPy nanocomposite and (2) NaDBS-doped polypyrrole-multi-walled carbon nanotube (PPy-MWCNT), as sensing materials in MEMS applications. The bulk and surface material properties, as well as electrical properties when integrated with MEMS electrodes, are characterized experimentally and the feasibility of using this material for hydrogen peroxide and glucose detection under the MEMS platform is demonstrated.

## 2. Design and fabrication

The earliest conductive polymer-based (either polyaniline or polypyrrole) conductimetric biosensors were developed for pH [14] and penicillin detection [15], and subsequently, research has also been carried out for glucose [16]. In conductimetry, only two electrode terminals are required for measurement, namely, the source and the drain terminals, as illustrated in figure 2(a). Sensing is effected via the changes in the conductance of the material that bridges the two terminals. Since the electrodes are to remain chemically inert within the range of the operating voltage or current, inert materials, e.g. gold, platinum or glassy carbon, are usually used. Moreover, depending on applications, the doping of the conductive polymer can be altered to produce either Schottky or Ohmic contact with the inert metal electrodes. Of the two types of contacts, Schottky contact at the metal/p-type conductive polymer interface tends to introduce more uncertainty in its output. Ohmic contact, on the other hand, gives more

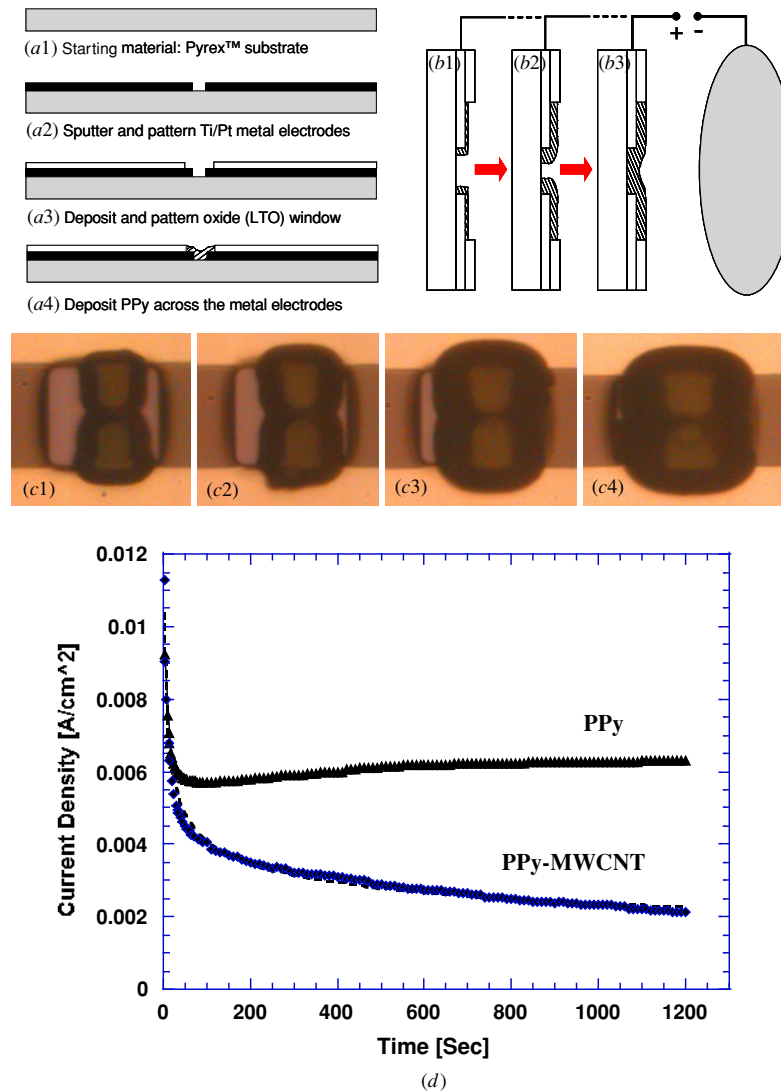


**Figure 3.** The wafer-level fabrication process of a PPy–MWCNT micro-gap sensor is illustrated in (a1)–(a4) while (b1)–(b3) show the electropolymerization process of PPy across the micro-gap. Panels (c1)–(c4) illustrate the chronopotentiostatic growth profile of the composite at 12 min, 15 min, 30 min and 40 min, to fill the  $8 \mu\text{m} \times 5 \mu\text{m}$  gap. (d) The chronoamperograms for a  $4000 \mu\text{m} \times 5 \mu\text{m}$  gap. The areas under the two curves (charge differential) translate into the deposited thicknesses of PPy and PPy–MWCNT.

reproducible results and hence is more desirable. To this end, platinum (Pt) is recommended for forming Ohmic contact with p-type conductive polymer such as PPy [4].

Figures 2(b)–(d) show schematics of a PPy conductimetric sensor, the detection mechanism and the fabricated device. Figures 2(b) and (d) illustrate the conceptual schematic view and an oblique SEM of a fabricated PPy–MWCNT sensor ( $4 \mu\text{m} \times 5 \mu\text{m}$  gap), where the sensing circuit comprises a pair of Pt line-electrodes separated by a  $5 \mu\text{m}$  gap. The micro-gap is connected by a layer of enzyme (glucose oxidase, GOx)-encapsulating, electropolymerized, NaDBS-doped PPy or PPy–MWCNT. A conductive sensing junction is formed across which most of the electric potential drop occurs. Figure 2(b) illustrates the glucose enzymatic reaction that produces hydrogen peroxide ( $\text{H}_2\text{O}_2$ ) as shown in equation (1), a strong oxidant which enhances the conductivity of PPy or PPy–MWCNT by injecting holes into the delocalized  $\pi$ -electron system in the polymer backbone.

Figures 3(a) and (b) outline the sensor fabrication processes. Line-shape electrodes made of noble metals (Ti/Pt) are first sputter deposited and patterned on  $\text{Si}_3\text{N}_4$ , supported on a p-type Si substrate. This is followed by the deposition and patterning (via  $\text{CF}_4$  plasma etching) of  $2000 \text{ \AA}$  of low-temperature oxide (LTO) to expose the  $5 \mu\text{m}$  gap for PPy or PPy–MWCNT electropolymerization. The wafer is subsequently immersed in a stable colloid that contains 0.1 M each of pyrrole (Py) monomers (Sigma Aldrich Inc.) and NaDBS (Sigma Aldrich Inc.), and 0.1% (wt) of MWCNT (Nanostructured & Amorphous Materials Inc.) well dispersed by sonication. DBS<sup>−</sup>, a common surfactant, acts both as a dopant for PPy and as an anticoagulant for MWCNT. Due to its hydrophobic nature, MWCNT tends to coagulate in polar solvents by means of hydrophobic–hydrophobic interaction [17]. PPy–MWCNT is next potentiostatically (+0.6 V) deposited onto the anode, followed by the physisorption of GOx (Sigma Aldrich Inc., EC 1.1.3.4, from *Aspergillus niger*,  $1.94 \text{ kU ml}^{-1}$ ) onto the polymer film. Figure 3(c) traces

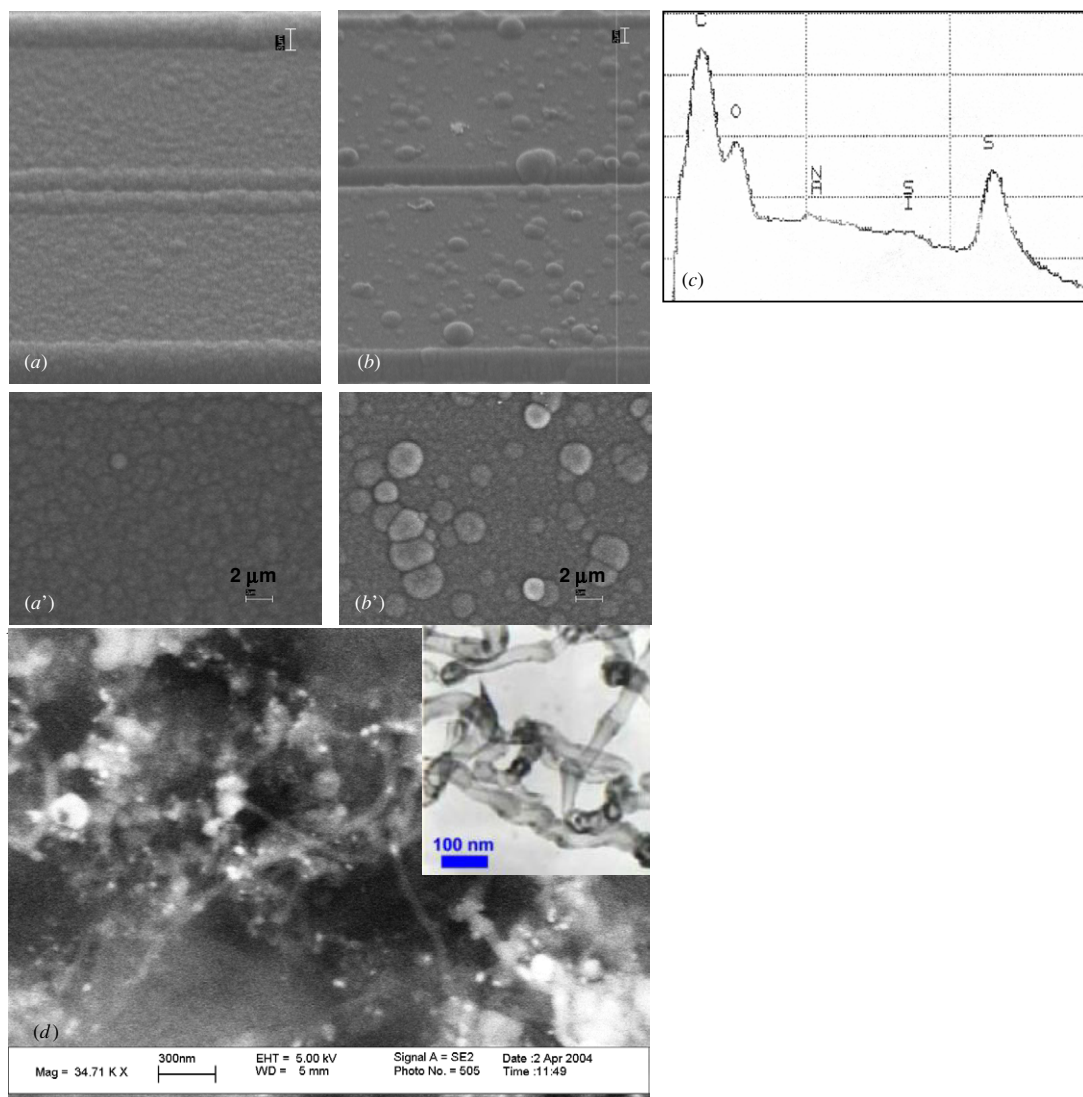


**Figure 4.** Panels (a and a') and (b and b') represent the top and the oblique SEMs of the surfaces of as-deposited PPy and PPy-MWCNT, respectively. (c) The electron dispersive spectrum of doped PPy shows the presence of Na and S peaks, which confirms the incorporation of NaDBS. (d) Cross-sectional view of the PPy-MWCNT polymer. Brighter spots represent non-conductive regions of the polymer. The inset shows the TEM of nanotubes as provided by the vendor.

the chronoamperometric growth profile of PPy-MWCNT which shows that the polymer grows in an isotropic fashion. Figure 3(d) gives the chronoamperograms showing the anodic current density profile of both PPy and PPy-MWCNT formation to seal a bridge gap of  $4000 \times 5 \mu\text{m}^2$ . As shown, during electropolymerization, both the current densities for PPy and PPy-MWCNT formation drop precipitously within the first 20 s. For PPy, the current density rebounds slightly and increases steadily beyond the first 20 s, and then stabilizes in the vicinity of  $6.25 \text{ mA cm}^{-2}$ . On the other hand, for PPy-MWCNT, the current showed no sign of stabilizing beyond the first 20 s. In fact, it continues to decrease steadily from  $5.7 \text{ mA cm}^{-2}$  (at 20 s) to  $2.1 \text{ mA cm}^{-2}$ , towards the end of the electropolymerization process. The areas under the curves indicate the amount of anodic charge injected during polymerization, which translates into the deposited thicknesses.

### 3. Characterization and discussions

#### 3.1. Blank, as-deposited PPy and PPy-MWCNT films

*3.1.1. Surface morphology and surface chemistry.* The growth of PPy is influenced by several factors that include the bias potential, electrode surface, solvent, pH of solution, dopants, temperature, presence of secondary entities such as nanoparticles, and solution agitation [4]. The PPy discussed here is synthesized in aqueous solution at room temperature, on an inert electrode surface (Pt), and in a quiescent environment. Figure 4 shows the scanning electron micrograph (SEM) and elemental composition (via electron dispersive spectrometry) of the as-deposited PPy and PPy-MWCNT films. In the absence of MWCNT, as illustrated in figures 4(a) and (a'), the surface roughness of PPy is relatively lower and the nodule sizes range from hundreds of nm up to  $1 \mu\text{m}$ . The addition of MWCNT, as pictured in figures 4(b) and (b'), favors the

formation of PPy nodules (up to  $\sim 3 \mu\text{m}$  in diameter) and increases the surface roughness of PPy-MWCNT. According to the SEMs, as-deposited, DBS-doped PPy and PPy-MWCNT films are electronically conductive, as evident from the lack of charge accumulation under the field-emission gun. When a PPy-MWCNT film is dissected to reveal its through-thickness structure, the embedded MWCNTs are exposed. Figure 4(c) is the electron dispersive spectrum of doped PPy which shows the presence of Na and S peaks, confirming the incorporation of NaDBS. From figure 4(d), the nanotubes are seen to be randomly distributed within the polymer matrix, which indicates the combination of sonication and surfactant ( $\text{DBS}^-$ ) helps stabilize the colloidal suspension and keeps the nanotubes well dispersed. Based on the micrograph, the diameters of these embedded nanotubes range from 40 to 100 nm. On the same SEM, the white regions indicate the insulating domains mentioned earlier, where charges built up under the microscope are not capable of being conducted away. This cross-section picture serves as a possible map on the distribution of conductive versus insulating regions within the polymer. The inset is the transmission electron micrograph (TEM) of MWCNT provided by the vendor [18]. From the TEM, the as-received nanotubes have an average diameter of  $\sim 40$  nm.

**3.1.2. Thickness and deposition rate measurements.** The thicknesses of the as-deposited films are measured by means of a profilometer (Alpha Step IQ Surface Profiler, KLA Tencor) and also via visual inspection under a scanning electron microscope. Measurements from both methods agree with results shown in figure 3(d), i.e., the thickness of PPy ( $\sim 4.1 \mu\text{m}$ ) corresponds approximately to twice the thickness of PPy-MWCNT ( $\sim 2.1 \mu\text{m}$ ) for a 20 min process. The deposition rates of the PPy and PPy-MWCNT are measured to be approximately  $0.2 \mu\text{m min}^{-1}$  and  $0.1 \mu\text{m min}^{-1}$ , respectively. It is generally known that the growth mechanism of PPy is very similar to that of metal vapor deposition or electrodeless metal plating [6]. In the early stages, the film starts to grow by an island-type nucleation on the electrode surface. The individual nuclei grow and enlarge, and at some point, they start to impinge on each other and coalesce to form a continuous film. In addition, for PPy, once the polymerization initiation phase is concluded, the subsequent propagation phase will proceed at a lower anodic potential, hence at a faster rate if the original applied potential is continued.

**3.1.3. Contact angle measurements.** Figure 5 illustrates the surface properties of PPy and PPy-MWCNT films of various thicknesses via a static sessile drop contact angle measurement. From the measurement data, it is observed that the films are hydrophilic by nature as the contact angles are below  $90^\circ$ . This may be expected since the lone pair of valence electrons in nitrogen could induce hydrogen bonding between the heterocyclic pyrrole and water molecules, which aids in the wetting of PPy as well as PPy-MWCNT. An interesting observation is that the contact angles increase with the PPy thickness, while the converse is true for PPy-MWCNT film, where there is a general decrease as film thickness increases. The presence of MWCNT provides more sites for nuclei formation such that there is more three-dimensional growth of

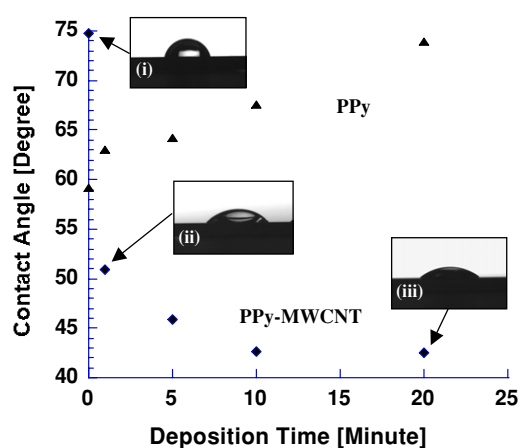


**Figure 5.** The contact angles of PPy and PPy-MWCNT. (i) This shows the water droplet on a hydrophilic gold surface ( $75^\circ$ ). (ii) and (iii) Water droplets with contact angles of  $51^\circ$  and  $42.5^\circ$  on PPy-MWCNT films that have undergone polymerization for 1 min ( $\sim 1000 \text{ \AA}$ ) and 20 min ( $\sim 2.1 \mu\text{m}$ ), respectively.

PPy and greater surface roughness as evident in figures 4(a) and (b). This could be one of the reasons that PPy-MWCNT film is more hydrophilic than the PPy film and further investigations on the surface roughness, interfacial energetics and capillary phenomenon [19] are required to provide better understanding.

### 3.2. As-deposited PPy and PPy-MWCNT devices

Two major types (based on width of electrodes) of PPy or PPy-MWCNT micro-gap sensors have been designed and fabricated for the proof-of-concept sensing demonstrations. Both types of sensors are made up of Pt electrode pairs separated by a fixed distance of  $5 \mu\text{m}$ . The 'narrow' micro-gap sensor has width dimensions of  $4 \mu\text{m}$ ,  $8 \mu\text{m}$ ,  $12 \mu\text{m}$  and  $16 \mu\text{m}$ , whereas the 'wide' micro-gap sensor has width dimensions of  $1000 \mu\text{m}$ ,  $2000 \mu\text{m}$  and  $4000 \mu\text{m}$ . Figure 6 juxtaposes the two types of sensors, with figure 6(a) being the wide micro-gap sensor and figure 6(b) being the narrow micro-gap sensor. Based on our experience in testing these sensors, wide micro-gap sensors tend to give more stable and reproducible responses, whereas narrow micro-gap sensors are somewhat less consistent in their outputs, especially with respect to the conductivity of the polymer and composite films. It is also observed that the growth profiles of PPy and PPy-MWCNT on a wide electrode are more uniform, with consistent thicknesses, as compared to a narrow electrode. This could largely be attributed to two effects. First, during the electropolymerization process, electric field tends to concentrate on sharp edges ('edge effect'), hence promotes non-uniform growth near the corners of the electrode. As film thickness increases, the edge effect becomes more prominent in a narrow micro-gap electrode as compared to a wide micro-gap electrode. Second, the average nodule size of the PPy is approximately of the order of  $1 \mu\text{m}$  and is of the same order of magnitude as the width of the narrow micro-gap electrode. Therefore, it is possible that small morphological change (variation in nodule sizes) could exert great influence on the electrical properties in the narrow micro-gap electrodes. This indicates that narrow electrodes are more

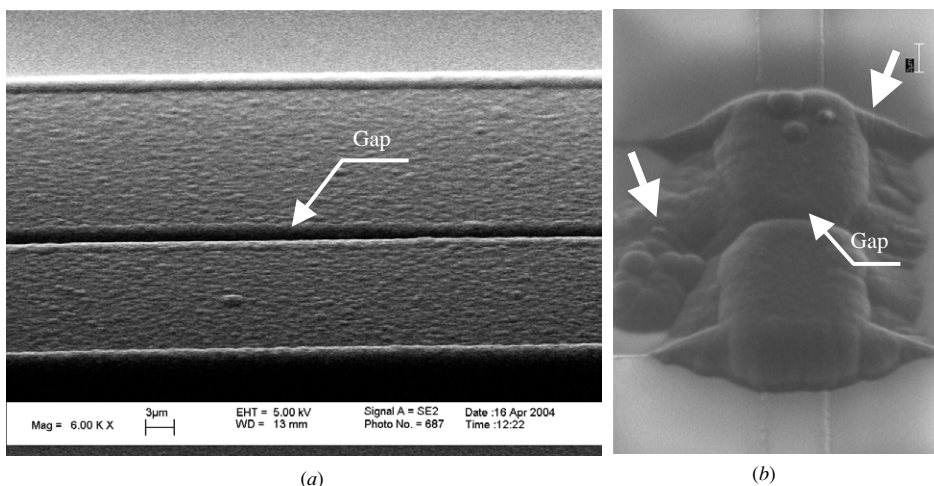


**Figure 6.** (a) A  $1000\ \mu\text{m} \times 5\ \mu\text{m}$  ‘wide’ micro-gap electrode and (b) a  $6\ \mu\text{m} \times 5\ \mu\text{m}$  ‘narrow’ micro-gap electrode. The white arrows in (b) indicate areas of non-uniform growth in a narrow micro-gap electrode.

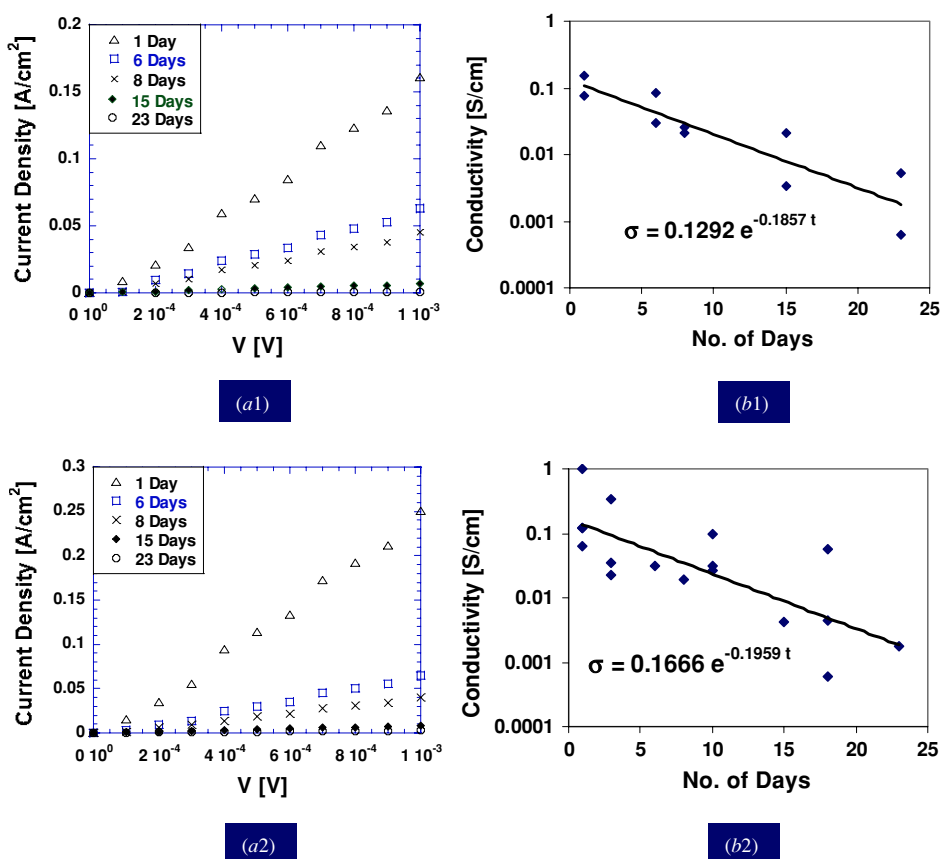


**Figure 7.** (a1 and a2)  $I$ – $V$  measurements show that both PPy and PPy–MWCNT membranes exhibit Ohmic behavior within the operational voltage range (0–1 mV). Reliability study of (b1) PPy (two devices) and (b2) PPy–MWCNT (four devices). As seen, the conductivities of both materials decrease over time.

sensitive to the fabrication conditions and the reproducibility of results rests heavily on good experimental control. We have characterized several properties of the deposited films, including  $I$ – $V$  characteristics, dc conductivity and preliminary glucose and hydrogen peroxide tests as presented below. Other studies such as gas diffusion on the composites in order to

determine porosity indices could be further developed to get a better understanding of these films.

**3.2.1.  $I$ – $V$  characteristics.** Figures 7(a1) and (a2) show the current–voltage ( $I$ – $V$ ) measurements of conductimetric sensors ( $4000\ \mu\text{m} \times 5\ \mu\text{m}$ ) made of PPy and PPy–MWCNT,

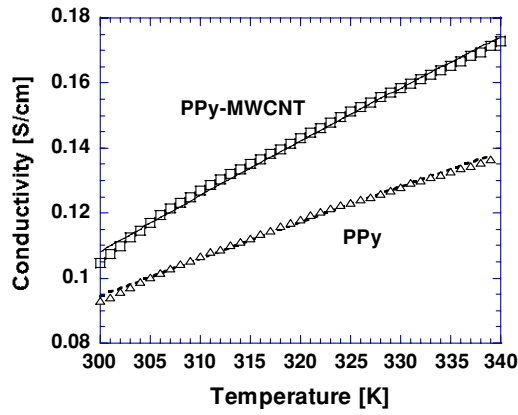


**Figure 8.** The conductivities of PPy and PPy-MWCNT increase with temperature.

respectively, over the course of 23 days in an ambient environment. The maximum operating voltage is set at 1 mV, corresponding to a maximum potential difference of  $200 \text{ V m}^{-1}$  over a  $5 \mu\text{m}$  gap, with ten potential steps each of  $100 \mu\text{V}$ . The  $I$ - $V$  graphs exhibit a linear current-voltage relationship, indicating that both PPy and PPy-MWCNT obey Ohm's law and behave like Ohmic materials within this operating voltage range. This is an advantage since the modeling of a PPy or a PPy-MWCNT conductimetric sensor is simplified based on an Ohmic response of the sensing materials. The current density (at 1 mV) of PPy-MWCNT ( $0.25 \text{ A cm}^{-2}$ ) is significantly higher than PPy ( $0.16 \text{ A cm}^{-2}$ ), 1 day after the deposition. However, the decay of PPy-MWCNT afterwards follows the same pattern as PPy and they decay to similar values. Figures 7(b1) and (b2) illustrate the temporal change of the dc conductivity of PPy and PPy-MWCNT in an ambient environment due to an irreversible degradation process known as 'aging'. Multiple factors contribute to aging, one of them being the presence of oxygen molecules, which is the most likely mechanism in our samples, as they are stored at ambient conditions. During the aging process, the insulating domains in the polymer matrix expand at the expense of the conducting domains. The dwindling proportion of conductive domains causes the hopping activity of charge carriers to decrease, as there are fewer conducting pathways available for the passage of these charge carriers [20].

**3.2.2. DC conductivity.** Figures 8(a)–(c) illustrate the effects of temperature and humidity on the dc conductivity of PPy and PPy-MWCNT. As shown in figure 8(a), we have characterized the temperature-dependent ambient condition response using wide electrodes ( $1000 \mu\text{m}$  wide  $\times$   $5 \mu\text{m}$  gap) bridged by PPy or PPy-MWCNT film (film thickness  $\sim 5 \mu\text{m}$ ). It is commonly known that the resistivities of semiconductors decrease with temperature as the number of charge carriers increases with temperature rise. On the other hand, for metals, resistivity increases with temperature due to phonon-induced scattering. As seen in figure 8, the dc conductivities of both PPy and PPy-MWCNT rise as temperature is raised from 300 to 340 K, indicating their structural resemblance to semiconductor. However, the difference in conductivities diverges, and widens from  $1.2 \times 10^{-2} \text{ S cm}^{-1}$  at room temperature to  $3.6 \times 10^{-2} \text{ S cm}^{-1}$  at 340 K. While the semiconducting properties

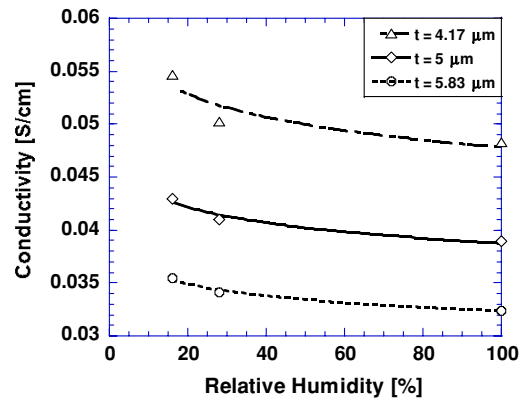


**Figure 9.** DBS-doped PPy is sensitive to various relative humidity (RH) levels at ambient temperature ( $t$  = PPy film thickness).

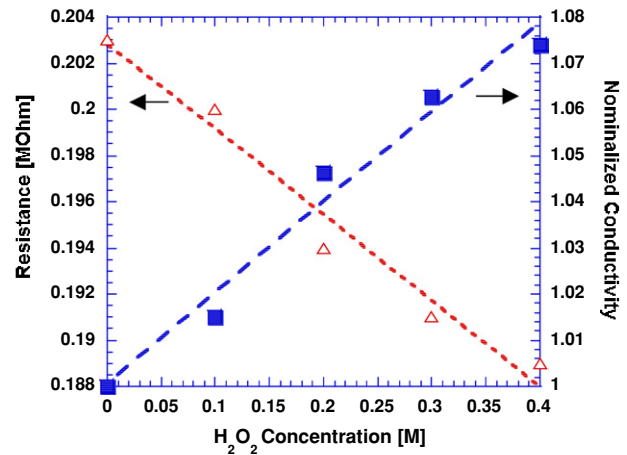


**Figure 10.** The nominalized conductivity of a micro-gap PPy-MWCNT sensor increases linearly as the concentration of  $\text{H}_2\text{O}_2$  increases.

of PPy have contributed to this increase, the effects of nanotubes require further characterization when a temperature differential arises. Unlike carbon fibers which have anisotropic thermal properties, carbon nanotubes have been demonstrated to expand isotropically when heated [21]. As mentioned earlier, mechanical stress/strain could affect the electrical properties of PPy and when the temperature gradually rises, thermal mismatch between PPy and MWCNTs could also contribute to the measured results.

Aside from temperature, humidity also has an effect on the conductivity of PPy, and PPy is capable of responding rapidly to humidity change, and does so in a reversible manner. Cassagnol *et al* [22] reported that the conductivities of PPy that are chemically (as opposed to electrochemically) doped with *p*-toluenesulfonic acid (PPy( $\text{PTS}^-$ )) and hydrogen sulfate (PPy( $\text{HSO}_4^-$ )) increase with relative humidity and plateau around their equilibrium values (11% for PPy( $\text{PTS}^-$ )) and 12% for PPy( $\text{HSO}_4^-$ )). From our experimental data, DBS-doped PPy behaves differently from chemically doped PPy( $\text{TS}^-$ ) or PPy( $\text{HSO}_4^-$ ). Figure 9 shows that, as humidity increases from 16% to 100%, the conductivity of DBS-doped PPy decreases. Quite evidently, the response of PPy to humidity is a function of the fabrication method (chemical polymerization versus electropolymerization) and the types of dopants incorporated.

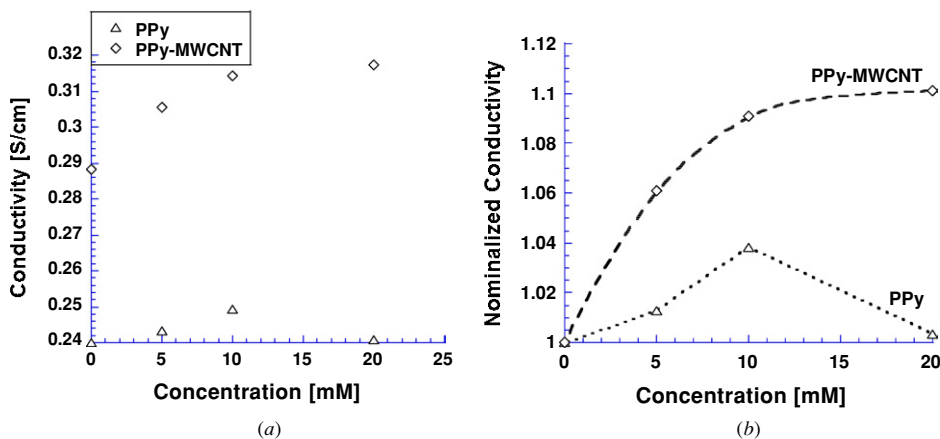


**Figure 11.** (a) Conductivity and (b) nominalized conductivity as a function of concentration. Both PPY and PPY–MWCNT sensors detect glucose, however, PPY–MWCNT exhibits a larger detection range (up to 20 mM) and also greater sensitivity ( $2.6 \times 10^{-3} \text{ S cm}^{-1} \text{ mM}^{-1}$ , compared to  $0.9 \times 10^{-3} \text{ S cm}^{-1} \text{ mM}^{-1}$  for PPY).

One observation is that the amplification factor can be altered via changing the dimensions of the electrodes and the gap, and the thickness of the polymer grown. Such a design guideline should be further established towards the construction of a sensitive humidity sensor.

**3.2.3. Glucose and hydrogen peroxide tests.** In the Clark-type or amperometric glucose sensing method [23], glucose molecules are detected at the enzyme-modified anode following enzymatic reaction with the glucose-specific redox enzyme, glucose oxidase (GOx). GOx is typically immobilized on the anode by means of physisorption, physical entrapment or covalent attachment. In the presence of oxygen, glucose ( $\text{C}_6\text{H}_{12}\text{O}_6$ ) is enzymatically oxidized at the anode to yield gluconolactone ( $\text{C}_6\text{H}_{10}\text{O}_6$ ) and hydrogen peroxide ( $\text{H}_2\text{O}_2$ ) according to the following equation:



We capitalize on the knowledge that PPY–MWCNT responds to oxidants such as  $\text{H}_2\text{O}_2$ , as shown in figure 10, to construct a two-terminal, GOx-encapsulated doped PPY–MWCNT glucose sensor. Conductivity change occurs when glucose reacts with the embedded enzymes and produces an oxidant,  $\text{H}_2\text{O}_2$ , which subsequently oxidizes the PPY by withdrawing electrons from (or injecting holes into) the  $\pi$ -conjugated system. This yields an output in the form of resistance change that can be recorded by means of a multimeter. Furthermore, the close proximity of GOx to the PPY network also ensures that electron mediators are not necessary, since electrons can readily come into contact with a conducting substrate, i.e. PPY matrix. Therefore, the sensor architecture obviates the need for a reference electrode as well as electron mediators, as electrons can be transferred in a direct, non-mediated fashion to the polymer.

Figure 11 juxtaposes the room-temperature conductivity and nominalized conductivity change of both PPY and PPY–MWCNT sensors ( $1000 \mu\text{m} \times 5 \mu\text{m}$  gap) at concentrations of  $\beta$ -D-glucose ranging from 0 to 20 mM. The sensors are initially immersed in de-ionized (DI) water (hence moisture does not play a role in the conductivity measurement) and subsequently subjected to glucose solutions of concentration

ranging from 5 mM to 20 mM. In between testing, the sensors are rinsed in copious amount of DI water. In the low detection range (0–5 mM), the conductivities of both sensors rise with increasing glucose concentration, with PPY–MWCNT attaining greater sensitivity ( $2.6 \times 10^{-3} \text{ S cm}^{-1} \text{ mM}^{-1}$ ) than PPY ( $0.9 \times 10^{-3} \text{ S cm}^{-1} \text{ mM}^{-1}$ ) based on the approximated linear response in this region. PPY–MWCNT shows signs of saturation beginning at 5 mM, where it transitions from a diffusion-controlled regime to an (enzyme) kinetics-controlled regime. On the other hand, PPY–MWCNT remains functioning up to 20 mM. It is well known that MWCNT are excellent in storing excess charges [24] for applications such as batteries and this should be the key factor in shielding the PPY backbone from losing its conductivity through overoxidation [12] as demonstrated by the experiments. The overall performance of these prototype devices is inferior to commercially available glucose sensors and only standard solutions were studied in this work. Therefore, it is necessary to conduct studies/developments on the optimization/testing of these devices in future works. Furthermore, we acknowledge that the reaction used for the sensing (i.e. the oxidation of the polypyrrole by hydrogen peroxide) is not selective enough to be used in a reliable glucose sensor and the proposed conductimetric sensor would most likely suffer from environmental factors such as temperature, humidity, stress, etc. The results presented in the paper, however, do provide a good foundation towards the development of reliable sensors utilizing compensation methodologies to minimize other environmental factors.

## 4. Conclusions

Room-temperature processed p-doped PPY–MWCNT nanocomposites potentially suitable for chemical and biomedical sensing applications have been developed and characterized. Based on the glucose and  $\text{H}_2\text{O}_2$  test results, the PPY–MWCNT nanocomposite exhibits an operating range up to 20 mM of glucose, which is a physiologically important range for diabetics. The addition of MWCNT into a PPY host matrix could help ameliorate the detrimental effect of overoxidation of the PPY polymer backbone. Since

it is possible to encapsulate different enzymes, the resulting bio-nanocomposite could potentially provide a new platform for the detection of other redox-based bio-molecules, such as metabolites, hormones and biotoxin. Capitalizing on the low cost and extrinsic (dopant- and redox-dependent) electrical properties of the PPy-MWCNT, it is believed that this class of nanocomposites could contribute to making point-of-care systems more affordable. However, it is noted that the presented sensing material is responsive to environmental factors such as temperature, humidity, stress, etc such that a designer must consider various compensation mechanisms to minimize the unwanted sensor responses.

## Acknowledgments

The authors would like to thank Hiu-Yung Wong, Sha Li and Firas Sammoura for assistance in device measurements, and Dr Yu-Chuan Su for valuable discussions on polymer. These devices were fabricated in the UC-Berkeley Microfabrication Laboratory and this work has been supported in part under a grant from the DARPA BioFlips program (F30602-00-2-0566) and an NSF award (ECS-0401356). KST is supported in part by an Eastman Kodak Fellowship.

## References

- [1] Smela E 1999 Microfabrication of PPy microactuators and other conjugated polymer devices *J. Micromech. Microeng.* **9** 1–18
- [2] Jager E W H, Smela E and Inganas O 2000 Microfabricating conjugated polymer actuators *Science* **290** 1540–5
- [3] Wong J Y, Langer R and Ingber D E 1994 Electrically conducting polymers can noninvasively control the shape and growth of mammalian cells *Proc. Natl Acad. Sci. USA* **91** 3201–4
- [4] Nalwa H S (ed) 2001 *Handbook of Surfaces and Interfaces of Materials: Biomolecules, Biointerfaces, and Applications* vol 5 (New York: Academic) chapter 11, pp 445–94
- [5] Smela E, Kallenbach M and Holdenried J 1999 Electrochemically driven polypyrrole bilayers for moving and positioning bulk micromachined silicon plates *J. Microelectromech. Syst.* **8** 373–83
- [6] Skotheim T A, Elsenbaumer R L and Reynolds J R 1998 *Handbook of Conducting Polymers* (New York: Dekker)
- [7] Orgzall I, Lorenz B, Dunsch L, Bartl A, Ting S T, Hor P-H and Hochheimer H D 1996 High-pressure low-temperature electrical properties of polypyrrole doped with *p*-toluenesulfonate *Synth. Met.* **81** 59–63
- [8] Teh K S and Lin L 2003 A micro-gap sensor based on conducting polypyrrole *Technical Digest: 7th Int. Conf. on Micro Total Analysis Systems (Squaw Valley, USA, 5–9 October)* pp 1195–8
- [9] Qian R, Pei Q and Li Y 1993 Proton doping of reduced polypyrrole *Synth. Met.* **61** 275–8
- [10] Gustafsson G, Lundstrom I, Liedberg B, Wu C R and Inganas O 1989 The interaction between ammonia and polypyrrole *Synth. Met.* **31** 163–79
- [11] Pfluger P, Krounbi M, Street G B and Weiser G 1983 The chemical and physical properties of pyrrole-based conducting polymers: the oxidation of neutral polypyrrole *J. Chem. Phys.* **78** 3212–8
- [12] Skotheim T A, Elsenbaumer R L and Reynolds J R 1998 *Handbook of Conducting Polymer* 2nd edn (New York: Dekker)
- [13] Yakushi K, Lauchlan L J, Clarke T C and Street G B 1983 Optical study of polypyrrole perchlorate *J. Chem. Phys.* **79** 4774–8
- [14] Thackeray J W and Wrighton M S 1986 Chemically responsive microelectrochemical devices based on platinumized poly(3-methylthiophene): variation in conductivity with variation in hydrogen, oxygen, or pH in aqueous solution *J. Phys. Chem.* **90** 6674–9
- [15] Nishizawa M, Matsue T and Uchida I 1992 Penicillin sensor based on a microarray electrode coated with pH-responsive polypyrrole *Anal. Chem.* **64** 2642–4
- [16] Bartlett P N and Birkin P R 1993 Enzyme switch responsive to glucose *Anal. Chem.* **65** 1118–9
- [17] Stevens R M, Nguyen C V and Meyyappan M 2004 Carbon nanotube scanning probe for imaging in aqueous environment *IEEE Trans. Nanobiosci.* **3** 56–60
- [18] <http://www.nanoamor.com/products>
- [19] Garbassi F, Morra M and Occhiello E 1994 *Polymer Surfaces: From Physics to Technology* (Chichester: Wiley)
- [20] Sixou B, Vautrin M, Attias A J and Travers J P 1997 Conductivity evolution of polypyrrole thin films with aging *Synth. Met.* **84** 835–6
- [21] Ruoff R S and Lorents D C 1995 Mechanical and thermal properties of carbon nanotubes *Carbon* **33** 925–30
- [22] Cassagnol C, Olivier P and Ricard A 1998 Influence of the dopant on the polypyrrole moisture content: effects on conductivity and thermal stability *J. Appl. Polym. Sci.* **70** 1567–77
- [23] Turner A P F, Karube I and Wilson G S (ed) 1987 *Biosensors, Fundamentals and Applications* (Oxford: Oxford University Press) chapter 13, p 211
- [24] Hughes M *et al* 2002 Electrochemical capacitance of nanocomposite films formed by coating aligned arrays of carbon nanotubes with polypyrrole *Adv. Mater.* **14** 382–5